Phase control of bouncing droplets and rearrangement of bound states

Davis J. Evans,[1] Bauyrzhan K. Primkulov,[2,1] and John W. M. Bush[1,*]
[1]*Department of Mathematics, MIT, Cambridge, Massachusetts 02139, USA*
[2]*Department of Mechanical Engineering, Yale University, New Haven, Connecticut 06511, USA*

(Received 28 May 2025; accepted 18 December 2025; published 23 January 2026)

The hydrodynamic pilot-wave system [Couder *et al.* Nature (London) **437**, 208 (2005)] consists of millimetric drops bouncing on the surface of a vibrating liquid bath. When the droplet's bouncing period is twice that of the vibrational forcing, it achieves resonance with its subharmonic Faraday wave field. The bouncing state may then destabilize into a walking state, in which the droplet self-propels, piloted by its own wave field. Since these Faraday waves are subharmonic with respect to the vibrational driving, there are necessarily two resonant bouncing or walking states, distinguished according to the droplet's impact phase relative to the bath vibration. The interaction between two or more bouncing droplets depends strongly on their relative phase. We here consider a bath driven concurrently by a primary oscillation and a secondary oscillation with half the frequency, and demonstrate that the imposition of the latter allows for controlled switching between the two resonant bouncing states. We demonstrate that when such a switch is applied to a stable lattice of bouncing droplets, the resulting phase changes of the droplets prompt the reconfiguration of the lattice. We further demonstrate that when the pilot wave of a walking droplet is sufficiently large, it may play the role of the secondary bath forcing applied here, prompting switching between the two resonant bouncing states. Our integrated experimental and theoretical study thus informs the behavior of walking droplets in a number of established hydrodynamic quantum analogs.

DOI: 10.1103/8z1k-c144

I. INTRODUCTION

When a liquid bath is subject to vertical vibration with acceleration $\gamma \sin(2\pi f t)$, it destabilizes to a field of subharmonic standing Faraday waves, with frequency $f/2$ and wavelength $\lambda_F = 2\pi/k_F$ prescribed by the water-wave dispersion relation, when the vibrational acceleration exceeds the Faraday threshold, $\gamma > \gamma_F$ [1]. Below this threshold, a millimetric liquid droplet may bounce indefinitely on the vibrating bath surface, owing to the sustenance of a thin intervening air layer during impact [2]. For γ just above the bouncing threshold $\gamma_B < \gamma_F$, the droplet will bounce with the driving period $T = 1/f$. For most drops in the parameter regime of interest [3,4], further increasing γ leads to the bouncing period doubling to a value $2T$, in which case the droplet achieves resonance with its subharmonic Faraday wave field. In this "period-doubled" or "resonant" state, the bouncing droplet serves as a localized source of weakly damped, circularly symmetric Faraday waves with the Faraday period $T_F = 2T$ [2]. Notably, these resonant states arise for $\gamma < \gamma_F$; thus, the waves are generated entirely by the bouncing droplet.

Resonant droplets may either bounce in place or, for vibrational accelerations γ above the "walking threshold" $\gamma_W > \gamma_B$, "walk" horizontally across the bath, propelled by their self-induced guiding or "pilot" wave [5]. The resonant bouncing state is denoted (2,1) in (m, n) notation, according to

*Contact author: bush@math.mit.edu

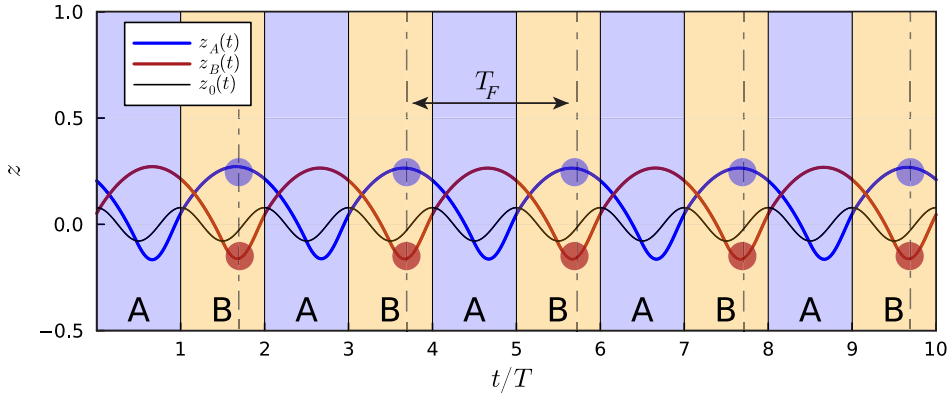

FIG. 1. Vertical dynamics of a bath surface vibrating at frequency $\omega = 2\pi/T$, and of resonant bouncing droplets. Vertical motion of the bath surface, $z_0(t)$ is indicated by the black curve. Trajectories of the two permissible states, $z_A(t)$ and $z_B(t)$, of resonant droplets bouncing at the Faraday frequency $\omega_F = \omega/2$ are indicated by blue and red curves, respectively. Bouncing states "A" and "B" differ only by a shift of time $t \mapsto t + T$, where $T = T_F/2$ is the driving period. State A refers to a droplet that bounces during odd periods of the driving (blue); likewise, B refers to droplets that bounce during even periods (red). The two states can be distinguished experimentally by means of a strobed illumination tuned to the Faraday frequency, $\omega_F = 2\pi/T_F$. Capturing images at the particular phase indicated by the vertical dashed lines will reveal states A and B at, respectively, the apex and nadir of their trajectories, so would be referred to as "up" and "down" states.

which a droplet bounces n times in m periods of bath vibration [2,6]. Since resonant droplets bounce at twice the driving period of the bath, $T_F = 2T$, two distinct periodic trajectories are admissible, that may be distinguished by their impact phase relative to the cycle of bath vibration [7]. The associated vertical droplet trajectories $z(t)$ and $z(t + \frac{T_F}{2})$ are shown in Fig. 1. Experimentally, the relative phase of droplets can be distinguished by strobed illumination at the Faraday period $2T$, which reveals one of two bouncing states that will appear at different points in their bouncing cycle. Once the phase of image capture is specified, such states may be referred to as "up" or "down." For example, image capture at the phase indicated in Fig. 1 coincides with states A and B being respectively "up" and "down."

The distinction between in- and out-of-phase droplets is particularly important in the dynamics of bound states, stable static or dynamic states of multiple droplets interacting through their mutual wave field [3]. Such bound states are of particular interest as they have provided the basis of hydrodynamic analogs of crystal lattices [8,9], spin lattices [10] and the bag model of the neutron [11]. Because reversing the impact phase of a droplet results in a sign reversal in the wave-induced force it experiences at impact, the equilibrium distance between neighboring droplets is sensitive to their relative phase. This distinction is encountered in the study of droplet lattices [8,9,12], stationary [13], ratcheting [14], orbiting [5,15] and promenading pairs [15,16], rings [17,18], and spin lattices [10] of bouncing droplets. In their study of Archimedean lattices, Eddi *et al.* [8] determined that the preferred equilibrium distances (or bond lengths) of neighboring bouncers are related to the Faraday wavelength λ_F by

$$d_n = (n - \varepsilon_F)\lambda_F, \tag{1}$$

where $\varepsilon_F = 0.2$, $n = 1, 2, 3, \ldots$ for in-phase droplets and $n = \frac{1}{2}, \frac{3}{2}, \frac{5}{2}, \ldots$ for out-of-phase droplets. A similar dependence was reported and rationalized in studies of stationary [13] and ratcheting [14] pairs. Equation (1) requires that altering the relative phase of neighboring bouncers precipitates the rearrangement of bound states.

In certain settings, the pilot-wave hydrodynamic system discovered by Yves Couder and Emmanuel Fort [5] has been shown to exhibit statistics comparable to those arising in microscopic,

quantum systems [19], and so has provided the basis for the field of hydrodynamic quantum analogs [20]. The quantum features are most pronounced in the "high-memory" limit arising as the vibrational acceleration approaches the Faraday threshold, $\gamma \to \gamma_F$, when the droplet's pilot-wave field, which serves as the system memory, is most persistent [21]. Phase flips of walking droplets have been reported in a number of settings. Perrard *et al.* [22] demonstrated that applying a "prescribed and controlled forcing" to the bath by temporarily increasing the driving acceleration γ to $\gamma + \Delta\gamma$ may cause a droplet to reverse its phase. This phase reversal was accompanied by a reversal in the horizontal direction of motion, and an erasure of the wave field, prompting the system to be described in terms of a wave-based Turing machine. Primkulov *et al.* [23] reported phase reversals at the onset of walking, and when walkers interact with a standing field of Faraday waves [24]. Droplets walking in a circular domain exhibit wave-like statistics in the histogram of droplet position, reminiscent of those in the quantum corral [25,26]. In the high-memroy regime in which quantum-like statistics emerge, the droplet is marked by sporadic sharp reversals in walking direction, indicative of phase flipping (Fig. 7) [23].

Sampara and Gilet [27] were the first to examine the influence of an additional forcing frequency in the bath vibration on the walking droplets. Specifically, they added a 64 Hz secondary signal to an 80 Hz primary signal and reported that chaotic horizontal droplet motion may then arise in the absence of confinement. Subsequently, Valani *et al.* [28] demonstrated that the application of two-frequency vibrational forcing supports 'superwalking' droplets, which can be considerably larger and faster than the traditional (2,1) walking droplets. These superwalkers emerge when the bath is driven by an acceleration $\gamma_p \sin(\omega t) + \gamma_s \sin(\omega t/2 + \Delta\phi)$, where γ_p denotes the primary acceleration at 80 Hz, γ_s the secondary acceleration at 40 Hz, and $\Delta\phi$ is the phase lag of the secondary component relative to the primary. In the experiments to be reported here, we similarly drive the bath with both primary and secondary oscillations, the secondary having half the frequency of the primary. Moreover, we fix the phase difference between primary and secondary vibrations to be $\Delta\phi = \pi/2$. Doing so allows for phase synchronization of bouncing droplets bound in a lattice that may induce a restructuring of the lattice. We also examine the role of phase flipping on walking droplets. Notably, selecting $\Delta\phi = \pi/2$ results in a local interfacial motion comparable to that of a Faraday wave of height $h_s = 4\gamma_s/\omega^2$. We thus regard the application of the secondary driving as a controlled way to simulate the presence of an anomalous pilot wave beneath the droplet.

In Sec. II, we present the results of our experimental exploration of the influence of secondary forcing on bouncing and walking droplets. Particular attention is given to the rearrangement of bound states of bouncing droplets, and the phase flipping and subsequent reversal of walkers prompted by the imposition of the secondary forcing. In Sec. III, we develop a mathematical model based on that of Molacek and Bush [6,7] for the case of a bath driven by both primary and secondary vibrations. We then perform a direct numerical simulation of the mathematical model to characterize how the vertical bouncing is altered by the secondary driving. In Sec. IV, we summarize our results and discuss hydrodynamic quantum analog systems where the phase flipping elucidated here may play a role.

II. EXPERIMENTS

We conduct all experiments on a vibrating bath of silicone oil ($\rho = 0.95$ g/ml, $\nu = 20$ cSt, $\sigma = 20.6$ mN/m) in an experimental apparatus described in Harris *et al.* [29] and illustrated in Fig. 2. Notably, this apparatus simply enables the application of two-frequency forcing, but does not allow for quantitative measurement of the magnitudes of the two vibrational accelerations. Drops are placed in a circular well (15 mm in radius), a relatively deep region (depth 6.5 mm) surrounded by a shallow layer (depth 0.5 mm) that serves to confine the drop to the deep region. We drive the bath with a primary vibrational forcing with peak acceleration γ_p and frequency $\omega = 2\pi f$, where $f = 80$ Hz (unless otherwise specified). In certain instances, we apply a secondary forcing with frequency $\omega/2$, peak acceleration γ_s, and phase shift $\Delta\phi = \pi/2$ relative to the primary forcing. We note that the apparatus used consists of a modified loudspeaker for which the input signal is

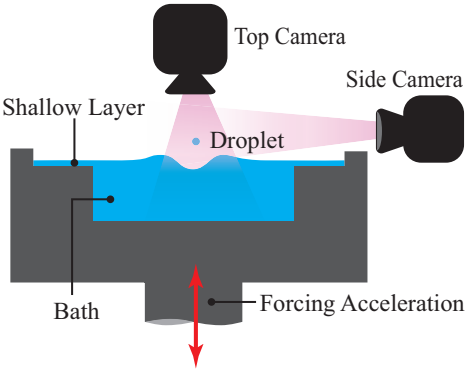

FIG. 2. Schematic of our experimental apparatus [29]. A bath of 20cSt silicone oil is driven vertically with a prescribed vibrational acceleration $\gamma_p \sin \omega t + \gamma_s \sin \omega t/2$. The deep region of the bath (depth 6.5 mm, diameter 3 cm) is surrounded by a shallow layer (depth 0.5 mm), thereby confining droplets to the deep region even if they transition to the walking state. The millimetric silicone oil droplets are imaged with both a side-profile camera and an overhead camera, each with an acquisition rate synchronized to a multiple of the Faraday period $T_F = 2\pi/\omega_F$.

supplied to the speaker/shaker through an audio jack [29]. The acceleration was adjusted by fixing the ratio of the two input audio signal amplitudes and varying the shaker volume. Because this setup does not allow for more precise control of the vibrational acceleration, we were constrained to qualitative rather than quantitative experiments. Nevertheless, they are sufficient to illustrate the phase-flipping behavior of interest here that is more fully characterized through our supporting theoretical developments.

We first illustrate how the addition of the secondary vibration influences the bouncing phase of period-doubled droplets in resonant bouncing states. Figure 3 shows a side-profile view of the synchronization of an irregular array of bouncing droplets upon introduction of the subharmonic driving component. In the presence of the primary vibrational forcing, both up and down states are supported. When the secondary forcing of sufficient amplitude is added, all droplets transform into the "A-up" state. The droplets remain in the "A-up" state even when the secondary forcing is eliminated, indicating hysteresis in the system.

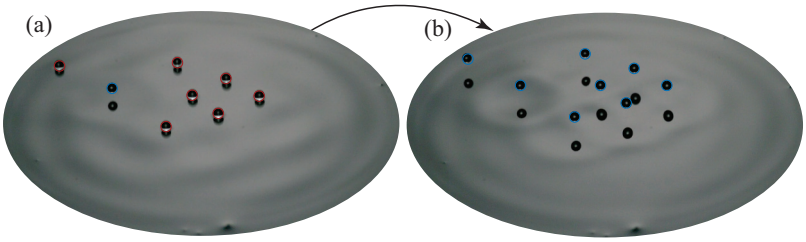

FIG. 3. An irregular assemblage of resonant bouncing droplets (radius $R = 0.37$ mm) is synchronized through imposition of a secondary forcing. Droplets in the "A-up" state are highlighted in blue to distinguish them from their reflections in the bath. Droplets in the "B-down" state are indicated in red. (a) When the bath vibration is forced at a single frequency ($f = 80$ Hz), with acceleration $\gamma \sin(\omega t)$, one drop in the "A-up" state bounces among seven drops in the "B-down" state. (b) When a secondary vibrational acceleration, $\gamma_s \cos(\omega t/2)$, is added with $\gamma_s = h\omega^2/4$ and phase difference $\Delta\phi = \pi/2$ relative to the primary driving, the same eight drops all assume the "A-up" state for $h > h^*$. See Video_FIG3 in the Supplemental Material [30].

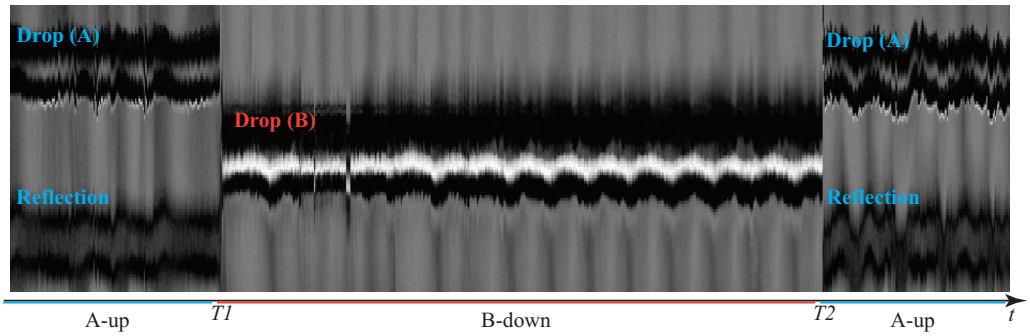

FIG. 4. Strobed kymograph of a bouncing droplet (radius $R = 0.37$ mm) switching between A (up) and B (down) bouncing states. The image was created by combining vertical slices taken along the droplet centerline, each 1 pixel wide, from consecutive strobed video frames captured at $\omega_F = \omega/8$, which corresponds to 9 frames per second. For $t < T_1$, the bath is forced at a single frequency ($f = \omega/2\pi = 72$ Hz) with acceleration $\gamma \sin(\omega t)$, and the droplet assumes the "A-up" state. Since the droplet bounces periodically (at the strobing and Faraday frequency), the droplet always appears at the same instant in its bouncing cycle, initially at the apex of its trajectory. (The lower stripe is due to the droplet's reflection in the bath, as is also apparent in Fig. 3.) At $t = T_1$, a secondary vibrational forcing is introduced at the half the frequency, yielding a bath acceleration $\gamma \sin(\omega t) + \frac{1}{4} h_s \omega^2 \cos(\omega t/2)$, with $h_s > 0$. The introduction of the secondary forcing prompts the droplet to transition to the "B-down" state, so that images are now captured at the nadir of the droplet's trajectory. At $t = T_2$, the sign of h_s is reversed to $h_s < 0$, which prompts a transition back to the "A-up" state. See Video_FIG4 in the Supplemental Material [30].

One can repeatedly flip the phase of a bouncing droplet by modulating the amplitude of the subharmonic forcing. This effect is demonstrated using the case of a single droplet. We drive the bath with two frequencies, yielding a net acceleration

$$a_b(t) = \gamma_p \sin(\omega t) + \gamma_s(t) \cos(\omega t/2), \tag{2}$$

where $\gamma_s(t) = h_s(t)\omega^2/4$ and $h_s(t)$ is the piecewise-constant amplitude of the secondary component of the bath vibration. We initiate the secondary driving at a prescribed time T_1 and then flip its sign after an interval $T_2 - T_1$; thus, $h_s(t) = 0$ for $0 < t < T_1$, $h_s(t) = h_0$ for $T_1 < t < T_2$, and $h_s(t) = -h_0$ for $t > T_2$. Figure 4 shows a kymograph of a droplet bouncing in place on a bath driven with the acceleration prescribed by Eq. (2). Note the phase flip resulting from the introduction of the secondary vibration at time T_1 and its subsequent reversal at T_2. Notably, droplets only undergo flips when h_0 exceeds a threshold h^*, and subsequently remain in that state when $h_s(t)$ is decreased back to zero, again indicating hysteresis in the system. When the secondary amplitude is reversed to $-h_0$, the drop again flips phases, restoring the "A-up" state.

Figure 5 illustrates the rearrangement of a pair of droplets prompted by the synchronization of their bouncing phase. The pair of droplets initially bounce out of phase with respect to each other, in a stable configuration with spacing $d_{3/2} \approx 1.3\lambda_F$ [2,13]. Introducing the secondary forcing provokes a synchronization of the bouncing phase, and concomitant adjustment to a new separation distance $d_1 \approx 0.8\lambda_F$, consistent with Eq. (1) when n changes from 3/2 to 1. The secondary forcing was applied as follows: $h_s(t)$ was increased from zero up to a value h_0 and promptly back down to zero following the phase flip.

Figure 6 shows a plan view of the rearrangement of a number of initially regular lattices. The top row shows a variety of lattices that owe their stability to the precise arrangement of in- and out-of-phase droplets. The middle row marks the point of phase synchronization of all droplets prompted by the introduction of the secondary forcing. The bottom row shows the emergent equilibrium configurations. While some of the emergent lattice structures are regular, others are not, and some are influenced by the presence of boundaries.

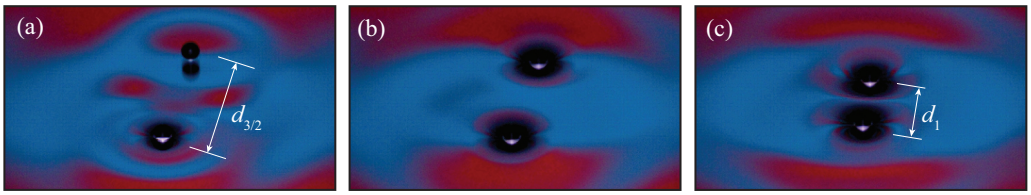

FIG. 5. A phase flip prompts the rearrangement of a stable pair of droplets with radius $R = 0.37$ mm driven at $f = 80$ Hz. (a) An out-of-phase pair at a distance $d_{3/2} \approx 1.3\lambda_F$ apart. (b) Immediately after the phase flip. (c) Rearrangement to a distance $d_1 \approx 0.8\lambda_F$, the preferred bond length for bound pairs of in-phase droplets, consistent with Eq (1). See Video_FIG5 in the Supplemental Material [30].

Figure 7 illustrates the spontaneous phase flipping that may arise for a walker in a circular corral, even when the bath is forced at a single frequency. At relatively low memory [Fig. 7(a)], the droplet maintains a constant bouncing phase. At higher memory [Fig. 7(b)], it executes a spontaneous phase flip and sharp change of direction, prompted by the interaction with its pilot wave. We here use an applied secondary vibration to play a role analogous to the pilot wave in altering the droplet dynamics.

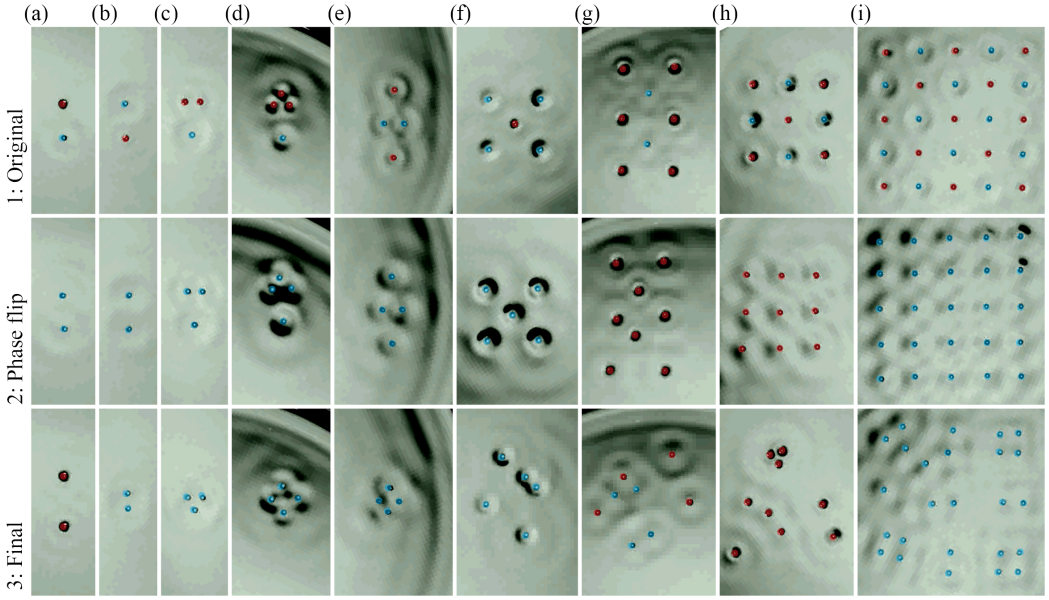

FIG. 6. Rearrangement of bound states of droplets with radius $R = 0.37$ mm driven at $f = 80$ Hz, due to an imposed secondary driving acceleration at 40 Hz. Because the preferred bond length depends on whether two droplets are in- or out-of-phase [see Eq. (1)], the synchronization in phase prompts rearrangement in lattices formed from in- and out-of-phase droplets. States (a)–(i) show different lattices with droplets in both the A-up (blue dot overlay) and B-down states (red dot overlay). Row 1 shows the initial stable configuration of a given bound states formed from both A-up and B-down droplets. Row 2 shows the synchronization of all droplets in a given lattice immediately following the introduction of the secondary driving acceleration, after the phase flip. Row 3 shows the new stable configurations of synchronized bouncers that emerge after the rearrangement. The asymmetry of some such configurations [e.g., (g), (i)] are due in part to the presence of boundaries. See Video_FIG6a-i in the Supplemental Material [30].

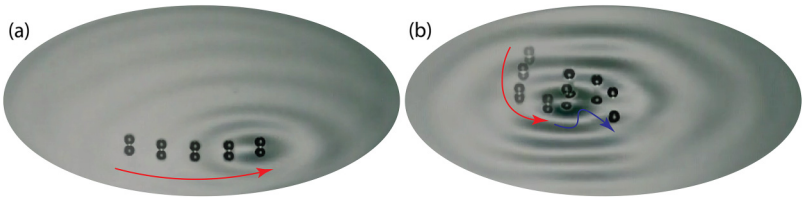

FIG. 7. Trajectory of the walker ($R = 0.37$ mm, $f = 80$ Hz) inside a circular corral at (a) low ($\gamma/\gamma_F \approx 0.91$) and (b) high memory ($\gamma/\gamma_F \approx 0.99$), when the bath is driven exclusively by the primary vibrational forcing. The arrow of time is indicated: more transparent drops correspond to earlier times. Strobed images are recorded at the subharmonic Faraday frequency so that different drop heights indicate different impact phases. In panel (a), the drop appears to glide along the bath in a down (blue) state. In panel (b), the drop flips to an up (red) state, prompted by interaction with its own pilot-wave field. See Video_FIG7a-b in the Supplemental Material [30].

III. THEORETICAL MODEL

We proceed by developing a theoretical model that allows us to rationalize the influence of the secondary vibrational forcing on the bouncing dynamics. The unperturbed interfacial height in the laboratory frame, $z_0(t)$, induced by both the primary and secondary driving of the bath (2), is

$$z_0(t) = h_p \sin(\omega t) + h_s \cos(\omega t/2), \tag{3}$$

where $h_p = \gamma_p/\omega^2$ and $h_s = 4\gamma_s/\omega^2$ are the amplitudes of the two components of the bath vibration. The vertical position of the droplet in the laboratory frame, $z = z(t)$, is governed by the force balance

$$m\ddot{z} = -mg + F_N. \tag{4}$$

Here, m is the droplet's mass, z is the droplet's vertical position, dots denote time derivatives, and $-mg$ is the downward force of gravity. $F_N = F_N(t)$ is the normal force applied to the drop by the bath, for which we adopt the theoretical model of Molacek and Bush [6,7],

$$F_N(t) = -(c(\dot{z} - \dot{z}_0(t)) + k(z - z_0(t)))\mathcal{H}(-(z - z_0(t))), \tag{5}$$

according to which the bath interface behaves like a linear spring with spring constant k (proportional to the surface tension [31]) and a linear dashpot with damping c. The presence of the Heaviside function $\mathcal{H}(x)$ in Eq. (5) ensures that $F_N(t)$ acts only during impact. Equation (5) has satisfactorily rationalized the myriad of bouncing and walking regimes arising when the bath is driven by a single frequency [4,6,7].

Equations (3)–(5) constitute the equations of vertical droplet motion. We now express the vertical dynamics relative to the unperturbed bath height $z_0(t)$ by defining the coordinate

$$Z = z - z_0(t). \tag{6}$$

The equation of motion thus transforms to

$$m\ddot{Z} + \mathcal{H}(-Z)(c\dot{Z} + kZ) = -mg + m\gamma_p \cos(\omega t) + m\gamma_s \sin(\omega t/2), \tag{7}$$

where the last two terms on the right-hand side constitute the fictitious force $-m\ddot{z}_0$ in the reference frame of the vibrating bath. We introduce dimensionless time $\bar{t} = t/T$ and length $\bar{Z} = Z/gT^2$, yielding the dimensionless equation

$$\bar{Z}'' + \mathcal{H}(-\bar{Z})\left(\frac{cT}{m}\bar{Z}' + \frac{kT^2}{m}\bar{Z}\right) = -1 + \frac{\gamma_p}{g}\cos(2\pi\bar{t}) + \frac{\gamma_s}{g}\sin(\pi\bar{t}). \tag{8}$$

Henceforth, we denote the dimensionless natural frequency by $\beta = \sqrt{\frac{kT^2}{m}}$, the dimensionless drag by $\zeta = \frac{1}{2\beta}cT/m$, the dimensionless primary driving acceleration by $\Gamma = \gamma_p/g$, and the

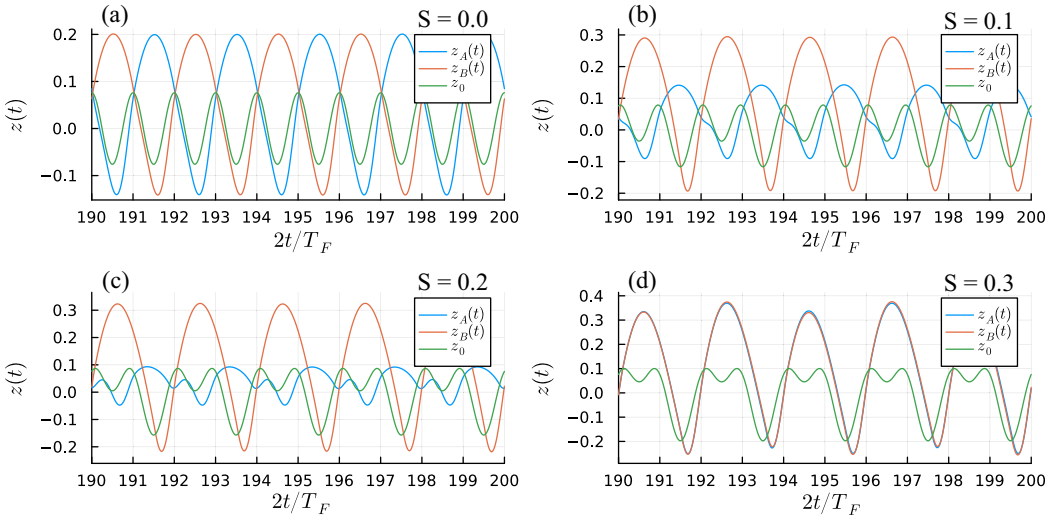

FIG. 8. Simulations characterize the influence of the dimensionless secondary driving acceleration S (over the range $0 \leqslant S \leqslant 0.3$) on vertical bouncing states A and B for $\Gamma = 3.0$, $\beta = 1.0$, and $\zeta = 0.33$. One state is initialized with $Z(0) = \dot{Z}(0) = 0$, the other with $Z(1) = \dot{Z}(1) = 0$. The vertical trajectories of the bath, and states A and B are reported in the laboratory frame. (a) For $S = 0$, states "A" and "B" differ only by a phase shift. (b) For $S = 0.1$ and (c) $S = 0.2$, the symmetry between states "A" and "B" is broken: "B" bounces significantly higher than "A." For S above a critical threshold (between 0.2 and 0.3), a trajectory originally in state "A" flips phase, while state "B" is largely unaffected. (d) For $S = 0.3$, there is thus only one accessible bouncing state: the degeneracy has been eliminated by the secondary forcing. The evolution toward this state is illustrated in Fig. 9.

dimensionless secondary driving acceleration by $S = \frac{\gamma_s}{g}$. We note that β is related to the drop vibration number introduced by Molacek and Bush [6,7]. Dropping overbars yields the dimensionless equation

$$\ddot{Z} + \mathcal{H}(-Z)(2\zeta\beta\dot{Z} + \beta^2 Z) = -1 + \Gamma\cos(2\pi t) + S\sin(\pi t). \tag{9}$$

We proceed by simulating Eq. (9) to characterize the symmetry breaking induced by the subharmonic driving. Equation (9) is solved numerically using a stiff ODE solver, specifically, the `Rosenbrock23()` method of the Julia library `DifferentialEquations.jl` [32]. Solutions in the complimentary states "A" and "B" are initialized by solving Eq. (9) with initial times that differ by one shaking period, thus, half a Faraday period. Specifically, we plot the steady states of two solutions obtained with parameters $\beta = 1$, $\Gamma = 3$, and $\zeta = 0.33$, one deduced from initial condition $Z(0) = \dot{Z}(0) = 0$, and the other from initial condition $Z(1) = \dot{Z}(1) = 0$. The symmetry of the two solutions "A" and "B" is evident in Fig. 8 for the case $S = 0$, but is broken by the introduction of the secondary vibration. In Fig. 8, we perform the same simulation but assign S to values of 0.1, 0.2, and 0.3. We note that the associated amplitudes of the secondary vibration are in the range 10–40 μm, consistent with characteristic pilot-wave amplitudes [33].

Figure 9 illustrates the evolution of the bouncing states predicted by Eq. (9) in response to abrupt changes in S, which serves to rationalize our experimental observations. When S is increased from 0 to 0.3, two states that are initially out-of-phase by one half-Faraday period respond differently. One state immediately increases its bouncing amplitude, reaching a new steady state; the other state slowly decreases its bouncing amplitude over approximately ten Faraday periods until it flips, then converges to the same steady state. When S is then reduced to 0, both states maintain the same bouncing phase.

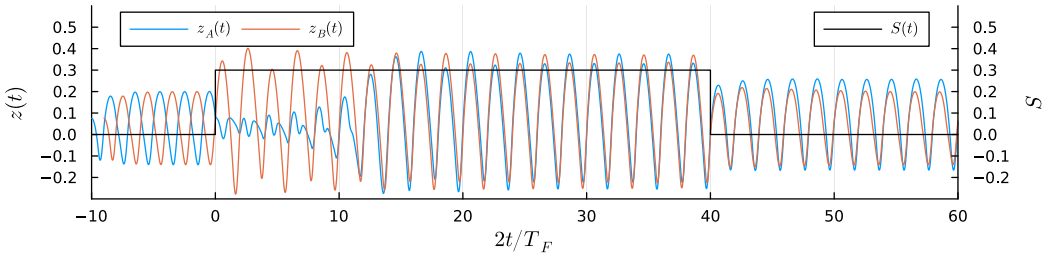

FIG. 9. Simulation characterizing the convergence of states "A" and state "B" in response to subharmonic forcing. Here, $\Gamma = 3.0$, $\zeta = 0.33$, $\beta = 1.0$. Initially, there is no subharmonic forcing $S = 0$. Initializing one state with $Z(-10) = \dot{Z}(-10) = 0$ and the other with $Z(-9) = \dot{Z}(-9) = 0$ gives rise to a pair of "A" and "B" states. At $t = 0$, S is abruptly increased to 0.3 prompting both A and B states to evolve to a new bouncing mode, eventually synchronizing to the state displayed in Fig. 8(d). At $t = 80T_F$, S is reduced to $S = 0$ and both solutions remain synchronized. We thus see the manner in which the degeneracy of the A and B states may be eliminated through application of subharmonic forcing.

We perform a preliminary parameter sweep and find that the choices of damping ratio $\zeta = 0.33$ and dimensionless natural frequency $\beta = 1$ predicts the period-doubling transition from (1,1) to (2,1) bouncing states at a value of $\Gamma \approx 2.2$ for $S = 0$ that is consistent with prior work [4,7]. We proceed by fixing ζ and β for the remainder of our study.

We characterize the steady attracting state of a given trajectory $z(t)$ by introducing the *steady-state average phase*

$$\Phi_\infty[z(t)] = \frac{\lim_{T\to\infty} \int_0^T F_N(t) \mathrm{mod}(\omega_F t, 2\pi) dt}{\lim_{T\to\infty} \int_0^T F_N(t) dt}, \tag{10}$$

where $F_N(t)$ is uniquely determined from Eq. (5). Note that Φ_∞ differs from the impact phase Φ defined in Molacek and Bush [6] in that Φ_∞ is defined relative to the Faraday period, while Φ was measured relative to the driving period. Moreover, Φ_∞ is calculated using a weighted average of the phase over an entire trajectory, while Φ characterizes a single bounce. This definition of Φ_∞ in Eq. (10) is necessary to distinguish between the A and B states; specifically, the phase Φ_∞ of droplets in states A and B shown in Fig. 1 differ by π. We proceed to perform a parameter sweep by examining Γ in the range $1.8 < \Gamma < 4.2$ and S in the range $-0.4 < S < 0.4$ and solving Eq. (9) for $z(t)$ with the initial conditions $Z(t_0) = 0$ and $\dot{Z}(t_0) = 0$ for t_0 in the range $0 < t_0 < 2T$. The solution $z(t)$ is simulated for a time $200T$ which we expect to be representative for computing Φ_∞.

Figure 10 shows the mean and variance of the steady-state impact phase Φ_∞ for a given choice of primary driving acceleration Γ and secondary driving acceleration S, as revealed through our simulations. The vertical centerline along $S = 0$ represents the case of no secondary forcing, and so may be compared to the behavior reported in prior studies concerned with monochromatic bath vibration [4,7,34]. For $\Gamma < 2.2$, periodic (1,1) or (2,2) bouncers may obtain; thus, the impact phase is unique, its standard deviation zero. For $\Gamma > 2.2$, both A and B resonant bouncing states are supported, leading to a large standard deviation in the impact phase. Application of the subharmonic forcing favors one state over the other, resulting in the triangular regions in Fig. 10(a) in which only one or the other is permissible. The range of S over which only A or B states are admissible decreases with increasing Γ. For $\Gamma > 4.0$, chaotic bouncing states emerge at the expense of the resonant states. The standard deviation in the bouncing phase is lowest in the regimes in which a single purely periodic bouncing state emerge, largest in regimes where states A and B coexist, and intermediate in the chaotic bouncing regime arising at high Γ.

Figures 10(c) and 10(d) show the dependence of the impact phase Φ_∞ on S for two particular values of Γ, corresponding to the two horizontal lines demarcated in Fig. 10(a). For $\Gamma < 2.2$, the

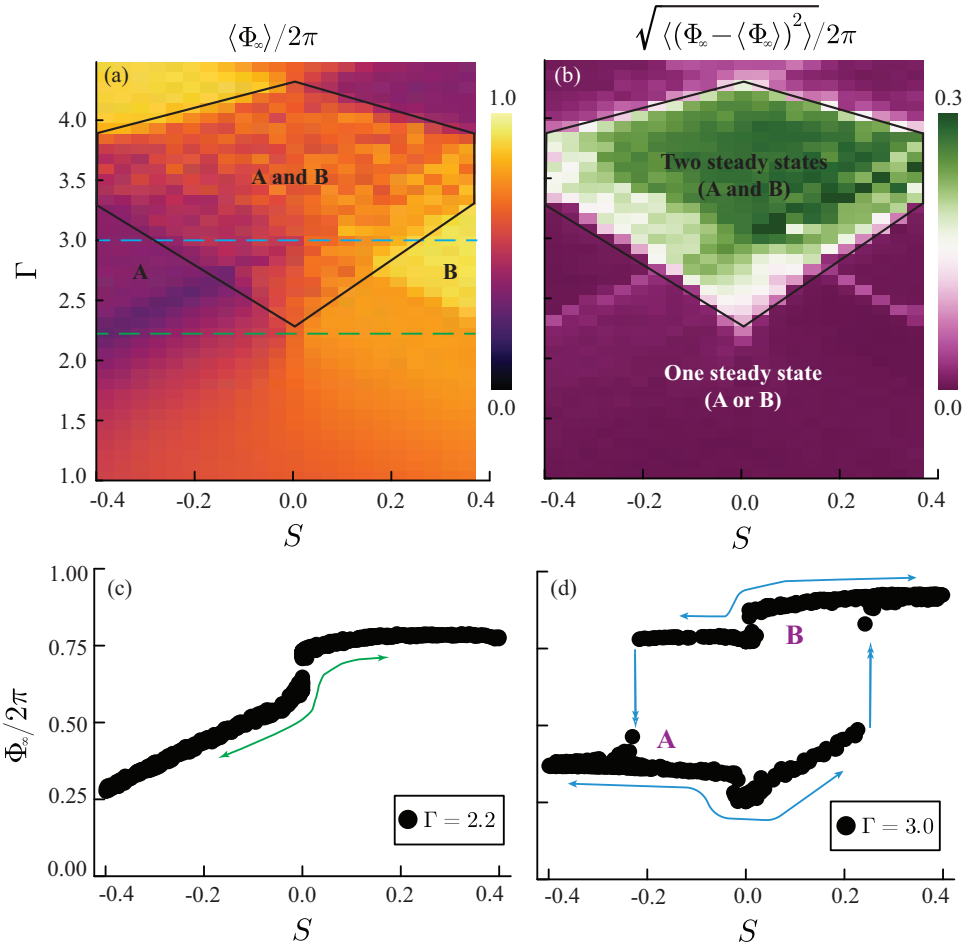

FIG. 10. (a) Mean and (b) variance of the steady-state average phase Φ_∞ obtained via direct numerical simulation of Eq. (9) for a particular choice of primary (Γ) and secondary (S) driving acceleration and $\beta = 1$ and $\zeta = 0.33$. The mean $\langle\Phi_\infty\rangle$ refers to an ensemble average over initial conditions $t_0 \in (0, 2\pi)$, likewise for the standard deviation $\sqrt{\langle\Phi_\infty - \langle\Phi_\infty\rangle\rangle^2}$. The partition of (Γ, S)-space where two steady states (both A and B) coexist are identified by the region with markedly higher standard deviation [green region in panel (b)]. Likewise, regions with near-zero standard deviation only accommodate one steady state (either A or B). Panels (c) and (d) display the dependence of Φ_∞ on S for fixed values of $\Gamma = 2.2$ and $\Gamma = 3.0$, respectively, corresponding to vertical lines in panel (a). For $\Gamma = 3$, two stable solutions, A and B exist for moderate values of $-2.2 < S < 2.2$.

phase is unique: the system supports only one steady state for any Γ_s. For larger Γ, the imposition of the secondary forcing γ_s introduces the possibility of two coexisting stable states (A and B), and an associated multivaluedness of the impact phase Φ. The paths taken by the system as S is increased, then decreased, are indicated for $\Gamma = 3$ in Fig. 10(d) and reflect the hysteresis in the system. Both paths are characterized by a spontaneous switch between states A and B at critical values of S. This hysteretic behavior is consistent with our experimental observations shown in Fig. 4.

IV. DISCUSSION

We have examined the dynamics of bouncing and walking droplets on a bath forced with two frequencies, a primary vibration and a secondary vibration with half the frequency. In so

doing, we have introduced a technique to control the bouncing phase resonant of bouncing and walking droplets. We have demonstrated that the introduction of the secondary driving may serve to synchronize the phase of all droplets on the bath. Moreover, hysteretic behavior of the phase in response to variation of the amplitude of the subharmonic driving allows droplets to persist in their phase-synchronized configuration even after elimination of the secondary driving. We expect that our method for phase synchronization will prove particularly beneficial in settings where such synchronization is difficult to achieve manually, as is the case for both Bravais lattices [9] and spin lattices [10].

We have simulated the vertical bouncing dynamics by adapting the theoretical model of Molacek and Bush [6,7] through inclusion of an additional subharmonic driving acceleration. In the absence of the secondary forcing, two stable solutions "A" and "B" exist that are identical up to a shift $t \mapsto t + T$ where $T = T_F/2$. Introducing secondary forcing with amplitude $S \neq 0$ breaks the symmetry between the two solutions, which may cause the loss of stability of one such solution for $S > S^*$ when S^* is a critical threshold that depends on Γ. We have characterized the stability boundary in (Γ, S) space numerically, as is summarized in Fig. 10.

In addition to demonstrating and rationalizing a method for control of the subharmonic phase of resonant bouncing droplets, our study provides insight into the phase-flipping dynamics of walking droplets apparent in a number of hydrodynamic quantum analogues. The anomalous interfacial height imposed by the secondary driving in our system was deliberately chosen to be comparable to the amplitude of a Faraday pilot wave arising at high memory. We thus expect that the phase flips prompted by the imposed secondary driving are similar to those of walkers prompted by interaction with their own pilot-wave field. Specifically, the range of S values reported in Fig. 10 correspond to wave amplitudes $h_s = \omega^2/(4\gamma_s)$ in the 10–40 micron range. By way of comparison, typical pilot-wave fields of free walkers are of magnitude 10 microns [33] but may be considerably larger for walkers approaching boundaries or confined to bounded domains.

Nonresonant effects and phase flips were the focus of a recent study by Primkulov *et al.* [23]. In a hydrodynamic analog of Kapitza-Dirac diffraction [24], droplets interacting with a standing Faraday wave were reported to undergo phase flips. Finally, similar phase flips have been reported for single droplets in the hydrodynamic corral [23,25], droplet pairs in neighboring wells [13], and free promenading pairs [15]. We suspect that the phase flips observed in these settings have occurred as a result of the pilot wave exceeding a critical threshold, so may be understood in the context of our study. An investigation of the role of nonresonant effects in general, and phase-flipping in particular, on the emergence of coherent quantum-like statistics, will be forthcoming.

ACKNOWLEDGMENTS

The authors gratefully acknowledge financial support from the National Science Foundation through Grant No. CMMI-2154151 and the Office of Naval Research through Grant No. N00014-24-1-2232.

DATA AVAILABILITY

The data supporting this study's findings are available within the article.

[1] J. Miles and D. Henderson, Parametrically forced surface waves, Annu. Rev. Fluid Mech. **22**, 143 (1990).

[2] S. Protière, A. Boudaoud, and Y. Couder, Particle–wave association on a fluid interface, J. Fluid Mech. **554**, 85 (2006).

[3] S. Protière, Y. Couder, E. Fort, and A. Boudaoud, The self-organization of capillary wave sources, J. Phys.: Condens. Matter **17**, S3529 (2005).

[4] O. Wind-Willassen, J. Moláček, D. M. Harris, and J. W. M. Bush, Exotic states of bouncing and walking droplets, Phys. Fluids **25**, 082002 (2013).
[5] Y. Couder, S. Protiere, E. Fort, and A. Boudaoud, Walking and orbiting droplets, Nature (London) **437**, 208 (2005).
[6] J. Moláček and J. W. M. Bush, Drops bouncing on a vibrating bath, J. Fluid Mech. **727**, 582 (2013).
[7] J. Moláček and J. W. M. Bush, Drops walking on a vibrating bath: Towards a hydrodynamic pilot-wave theory, J. Fluid Mech. **727**, 612 (2013).
[8] A. Eddi, A. Decelle, E. Fort, and Y. Couder, Archimedean lattices in the bound states of wave interacting particles, Europhys. Lett. **87**, 56002 (2009).
[9] M. M. Couchman, D. J. Evans, and J. W. M. Bush, The stability of a hydrodynamic bravais lattice, Symmetry **14**, 1524 (2022).
[10] P. J. Sáenz, G. Pucci, S. E. Turton, A. Goujon, R. R. Rosales, J. Dunkel, and J. W. M. Bush, Emergent order in hydrodynamic spin lattices, Nature (London) **596**, 58 (2021).
[11] R. N. Valani and D. M. Paganin, Active wave-particle clusters, Phys. Rev. E **112**, 065103 (2025).
[12] A. Eddi, A. Boudaoud, and Y. Couder, Oscillating instability in bouncing droplet crystals, Europhys. Lett. **94**, 20004 (2011).
[13] M. M. Couchman, S. E. Turton, and J. W. Bush, Bouncing phase variations in pilot-wave hydrodynamics and the stability of droplet pairs, J. Fluid Mech. **871**, 212 (2019).
[14] C. Galeano-Rios, M. Couchman, P. Caldairou, and J. W. Bush, Ratcheting droplet pairs, Chaos **28**, 096112 (2018).
[15] J. Arbelaiz, A. U. Oza, and John W. M. Bush, Promenading pairs of walking droplets: Dynamics and stability, Phys. Rev. Fluids **3**, 013604 (2018).
[16] C. Borghesi, J. Moukhtar, M. Labousse, A. Eddi, E. Fort, and Y. Couder, Interaction of two walkers: Wave-mediated energy and force, Phys. Rev. E **90**, 063017 (2014).
[17] M. M. P. Couchman and J. W. M. Bush, Free rings of bouncing droplets: Stability and dynamics, J. Fluid Mech. **903**, A49 (2020).
[18] S. J. Thomson, M. Durey, and R. R. Rosales, Collective vibrations of a hydrodynamic active lattice, Proc. R. Soc. A **476**, 20200155 (2020).
[19] J. W. M. Bush, Pilot-wave hydrodynamics, Annu. Rev. Fluid Mech. **47**, 269 (2015).
[20] J. W. M. Bush and A. U. Oza, Hydrodynamic quantum analogs, Rep. Prog. Phys. **84**, 017001 (2020).
[21] A. Eddi, E. Sultan, J. Moukhtar, E. Fort, M. Rossi, and Y. Couder, Information stored in faraday waves: The origin of a path memory, J. Fluid Mech. **674**, 433 (2011).
[22] S. Perrard, E. Fort, and Y. Couder, Wave-based turing machine: Time reversal and information erasing, Phys. Rev. Lett. **117**, 094502 (2016).
[23] B. K. Primkulov, D. J. Evans, J. B. Been, and J. W. M. Bush, Nonresonant effects in pilot-wave hydrodynamics, Phys. Rev. Fluids **10**, 013601 (2025).
[24] B. K. Primkulov, D. J. Evans, V. Frumkin, P. J. Sáenz, and J. W. M. Bush, Diffraction of walking drops by a standing Faraday wave, Phys. Rev. Res. **7**, 013226 (2025).
[25] D. M. Harris, J. Moukhtar, E. Fort, Y. Couder, and J. W. M. Bush, Wavelike statistics from pilot-wave dynamics in a circular corral, Phys. Rev. E **88**, 011001(R) (2013).
[26] P. J. Sáenz, T. Cristea-Platon, and J. W. M. Bush, Statistical projection effects in a hydrodynamic pilot-wave system, Nat. Phys. **14**, 315 (2018).
[27] N. Sampara and T. Gilet, Two-frequency forcing of droplet rebounds on a liquid bath, Phys. Rev. E **94**, 053112 (2016).
[28] R. N. Valani, A. C. Slim, and T. Simula, Superwalking droplets, Phys. Rev. Lett. **123**, 024503 (2019).
[29] D. M. Harris, J. Quintela, V. Prost, P.-T. Brun, and J. W. M. Bush, Visualization of hydrodynamic pilot-wave phenomena, J. Visualization **20**, 13 (2017).
[30] See Supplemental Material at http://link.aps.org/supplemental/10.1103/8z1k-c144 for videos.
[31] T. Gilet and J. W. M. Bush, The fluid trampoline: Droplets bouncing on a soap film, J. Fluid Mech. **625**, 167 (2009).
[32] C. Rackauckas and Q. Nie, DifferentialEquations.jl—A performant and feature-rich ecosystem for solving differential equations in Julia, J. Open Res. Software **5**, 15 (2017).

[33] A. P. Damiano, P.-T. Brun, D. M. Harris, C. A. Galeano-Rios, and J. W. M. Bush, Surface topography measurements of the bouncing droplet experiment, Exp. Fluids **57**, 163 (2016).

[34] P. A. Milewski, C. A. Galeano-Rios, A. Nachbin, and J. W. M. Bush, Faraday pilot-wave dynamics: Modelling and computation, J. Fluid Mech. **778**, 361 (2015).